254–261 *Nucleic Acids Research, 2006, Vol. 34, No. 1*
doi:10.1093/nar/gkj428

Structural and dynamic basis of a supercoiling-responsive DNA element

Sung-Hun Bae, Sang Hoon Yun[1], Dawei Sun, Heon M. Lim[1] and Byong-Seok Choi*

Department of Chemistry, KAIST, 373-1 Guseong-dong Yuseong-gu Daejeon 305-701, Republic of Korea and [1]Department of Biology, School of Biological Science and Biotechnology, Chungnam National University, Daejeon 305-764, Republic of Korea

Received July 2, 2005; Revised and Accepted December 15, 2005

ABSTRACT

In both eukaryotes and prokaryotes, negative supercoiling of chromosomal DNA acts locally to regulate a variety of cellular processes, such as transcription, replication, recombination and response to environmental stresses. While studying the interaction between the Hin recombinase and mutated versions of its cognate DNA-binding site, we identified a mutated DNA site that binds Hin only when the DNA is supercoiled. To understand the mechanism of this supercoiling-responsive DNA site, we used NMR spectroscopy and fluorescence resonance energy transfer to determine the solution structures and dynamics of three related DNA oligonucleotides. The supercoiling-responsive DNA site formed a partially unwound and stretched helix and showed significant flexibility and base pair opening kinetics. The single CAG/CTG triplet contained in this DNA sequence displayed the same characteristics as do multiple CAG/CTG repeats, which are associated with several hereditary neuromuscular diseases. It is known that short DNA sequence motifs that have either very high or low bending flexibility occur preferentially at supercoiling-sensitive bacterial and eukaryotic promoters. From our results and these previous data, we propose a model in which supercoiling utilizes the intrinsic flexibility of a short DNA site to switch the local DNA structure from an inefficient conformation for protein binding to an efficient one, or vice versa.

INTRODUCTION

The chromosomal DNA of both eukaryotes and prokaryotes is negatively supercoiled, either by the wrapping of DNA around histone proteins or by the topological constraints imposed upon closed circular DNA, respectively. Supercoiling plays an important role in a variety of cellular processes, including transcription, replication, recombination and response to environmental stresses (1,2). Global supercoiling changes are known to act locally and regulate the transcription of genes with promoters that are sensitive to supercoiling (~7% of the *Escherichia coli* genome) (3). Although the mechanism by which global supercoiling alters local DNA structure is not clearly understood, it is well known that many proteins bind preferentially to supercoiled rather than relaxed or linear DNA. In addition, it has been shown that changes in protein binding affinity and/or specificity induced by supercoiling are dependent on the local DNA sequence [e.g. (4)].

In our study of the DNA recombinase Hin from *Salmonella typhimurium*, we observed supercoiling-induced local structural changes in the Hin DNA-binding site. Hin catalyzes a site-specific DNA inversion between two 26 bp inverted sequences (*hixL* and *hixR*) that flank a 933 bp DNA segment. This invertible segment contains a promoter that directs the coordinate expression of the *fljB* and *fljA* genes, which encode H2 flagellin and a repressor of the H1 flagellin gene (*fljC*), respectively. By inverting this 933 bp segment, Hin regulates the expression of two major flagellar structural proteins, the H1 and H2 flagellins, which allow the bacteria to escape the host's immune system (5). During the first stage of DNA inversion, Hin binds to each of the 26 bp *hix* DNA sites as a dimer with high affinity ($K_d \sim 10^{-9}$) (6). It has been suggested that the specificity of Hin binding results from direct or water-mediated sequence-specific contacts made by the Hin protein with the major groove at positions 9–13 and with the minor groove at positions 5–6 (numbering from the center of the inverted sequence, Figure 1A) (7,8). However, in the present study, we show that (i) a DNA mutation at the central positions (+1,−1) of the *hix* site also modulates Hin binding and (ii) the mutated *hix* site, which does not bind Hin when the DNA is relaxed, can bind Hin when the DNA is in a supercoiled state. The negative supercoiling is required for

*To whom correspondence should be addressed. Tel: +82 42 869 2828; Fax: +82 42 869 8120; Email: byongseok.choi@kaist.ac.kr
Correspondence may also be addressed to Heon M. Lim. Tel: +82 42 821 6276; Fax: +82 42 822 9690; Email: hmlim@cnu.ac.kr

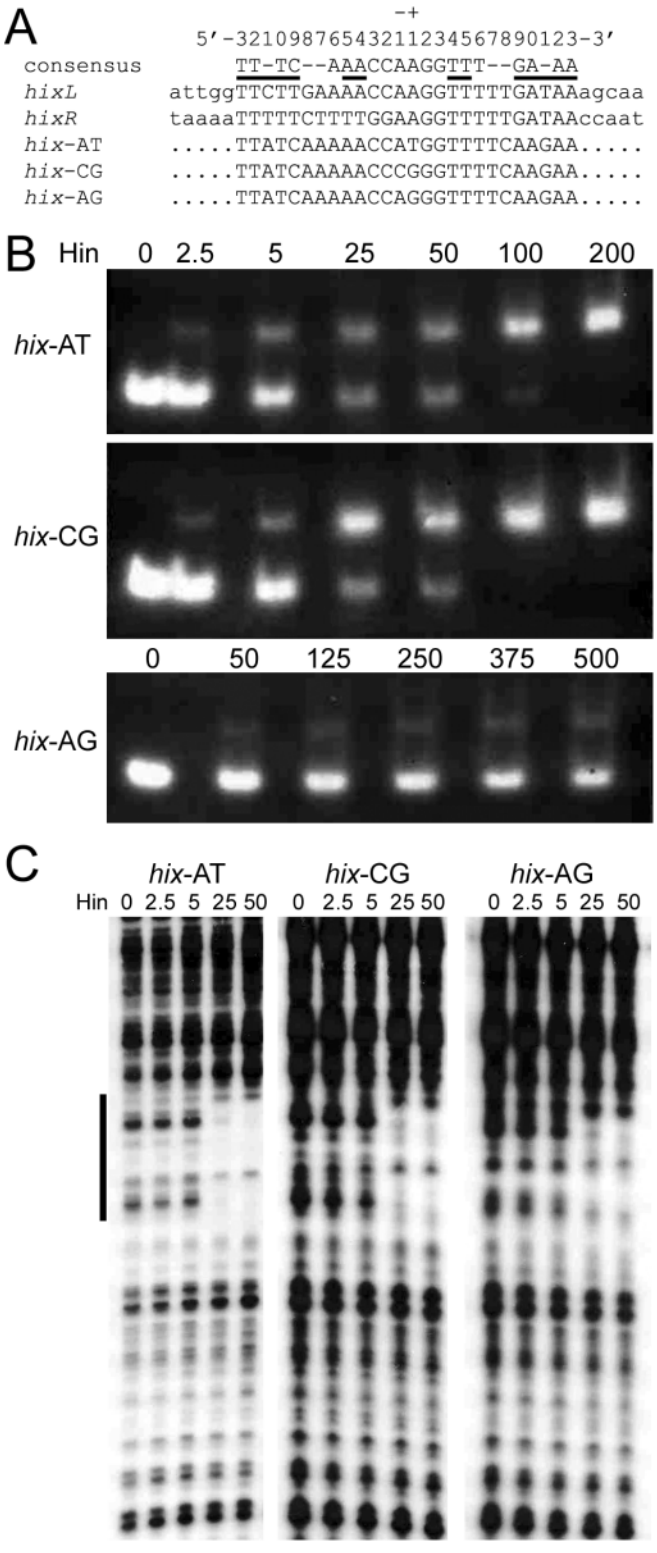

Figure 1. Supercoiling-dependent Hin binding to *hix*-AG. (**A**) DNA-binding sites (*hixL* and *hixR*) of the Hin recombinase from *S.typhmurium* and the mutant *hix* sites used in this study (*hix*-AT, *hix*-CG and *hix*-AG). Residues involved in sequence-specific contacts with Hin are marked by horizontal lines. (**B**) EMSAs with the 200 bp PCR-amplified DNA containing mutant *hix* sites (0.8 nM) and 0–200 or 500 ng/μl of the Hin protein. (**C**) DNase I footprinting of supercoiled plasmids containing mutated *hix* sites in the presence of the Hin protein (0–50 ng/μl). Protected region from DNase I digestion is indicated by a vertical bar in the left.

formation of the complete Hin inversion complex (9,10); however, it is not necessary for the initial recognition of the *hix* site by Hin (6,11). Therefore, the supercoiling-induced Hin binding observed in our study is solely caused by the properties of the mutated DNA site and hence provides a model of DNA site that responds to supercoiling.

To characterize this supercoiling-responsive DNA site, we have determined the solution structures and dynamics of three *hix*-related DNA oligonucleotides by NMR spectroscopy and fluorescence resonance energy transfer (FRET). Our results show that the supercoiling-responsive mutant *hix* site has a partially unwound and stretched helix structure and shows significant flexibility and base pair opening kinetics. The single CAG/CTG triplet contained in the supercoiling-responsive *hix* site displayed the same characteristics as CAG/CTG repeats, which are associated with several hereditary neuromuscular diseases such as myotonic dystrophy and Huntington's disease (12). Our results suggest that supercoiling affects predominantly the highly flexible DNA site and that such changes can switch the local DNA structure from an inefficient conformation for protein interaction to an efficient one, or vice versa.

MATERIALS AND METHODS

Hin protein preparation

Wild-type and G102A mutant Hin proteins were expressed and purified as described previously (13).

Electrophoretic mobility shift assay (EMSA)

PCR-amplified, 200 bp, double-stranded DNA (dsDNA) fragments containing the *hix*-AT, *hix*-AG and *hix*-CG sites were end-labeled with T4 polynucleotide kinase and [γ-^{32}P]ATP. Binding mixtures (20 μl) containing 0.8 nM of labeled DNA and 0–200 ng of Hin protein in binding buffer [0.2 M Tris–HCl (pH 7.5), 1 M NaCl, 10 mM EDTA, 100 mM DTT and 50 mM $MgCl_2$] were incubated for 10 min at 25°C. The mixtures were subjected to electrophoresis on 5% polyacrylamide gels.

DNase I footprinting

Supercoiled plasmid DNA (20 nM) containing the *hix*-AT, *hix*-AG and *hix*-CG sites were pre-incubated with 0–50 ng of Hin protein in 50 μl of the binding buffer for 10 min at 25°C. After the addition of 1 U of DNase I, the incubation was continued for 2 min. The digested DNA was isolated by phenol/chloroform extraction and extended with a ^{32}P-end-labeled primer. The extension products were separated on an 8% polyacrylamide/7 M urea gel.

NMR experiments

DNA oligonucleotides for NMR experiments were purchased from Bioneer Co., Ltd. (Daejeon, Korea). Buffer conditions for the NMR experiments were 10 mM sodium phosphate (pH 6.8) and 100 mM NaCl. All NMR spectra were obtained on a Varian Inova 600 MHz spectrometer except for the ^{1}H-^{31}P heteronuclear correlation spectra, which were acquired on a Bruker DRX 600 MHz spectrometer. The 2D NOE spectroscopy (NOESY) (τ_m = 180 ms) was carried out in 95% H_2O/5% D_2O at 4°C. The 2D NOESY (τ_m = 80, 160 and

240 ms), 2D correlation spectroscopy (COSY), 2D total correlation spectroscopy (TOCSY) ($\tau_m = 80$ ms) and ^1H-^{31}P heteronuclear COSY were conducted in 100% D_2O at 22°C. All the acquired spectra were processed by NMRPipe (14) and analyzed by Sparky 3 (T. D. Goddard and D. G. Kneller, University of California, San Francisco).

Resonance assignments and structure calculation

All of the slowly exchanging imino and amino resonances were assigned with the H_2O NOESY, and all non-exchangeable base and most of the sugar proton resonances were assigned by using the D_2O NOESY and TOCSY spectra. The distance constraints were derived from the integrated NOE peak volumes and three assumed isotropic correlation times ($\tau_c = 3$, 4 and 5 ns) using a relaxation matrix analysis program, MARDIGRAS (15). The δ dihedral angles were derived from the H1′-H2′ scalar couplings from regular 2D COSY (16). The χ dihedral angles were constrained to 220 ± 45°, on the basis of the medium to weak intra-residue NOE between H6 or H8 and H1′. The α and ζ angles were unconstrained, and other backbone dihedral angles were loosely constrained to the standard B-form [β (180 ± 45°), γ (60 ± 30°), ε (230 ± 70°)]. All the structure calculations were carried out using XPLOR-NIH (17). Two extended single DNA strands were used as a starting structure and were subjected to 60 ps of torsion angle dynamics (TAD) at 20 000 K, followed by 150 ps of TAD cooling from 20 000 to 0 K. The final structures were obtained after 20 000 cycles of energy minimization. The distance force constant was 50 kcal $mol^{-1}\cdot A^{-2}$ throughout the calculation and the dihedral angle force constant, which initially was 5, was scaled to 250 kcal $mol^{-1}\cdot rad^{-2}$ during cooling. The database potential of mean force base–base positional interactions was adopted with a force constant of 0.1 (18). For self-complementary DNAs (*hix*-AT and *hix*-CG), a non-crystallographic symmetry force constant of 10 was used. From 100 starting structures, 25, 15 and 13 structures for *hix*-AT, *hix*-CG and *hix*-AG, respectively, were converged to root mean square deviations (r.m.s.d.) of 0.56 ± 0.29, 0.61 ± 0.34 and 0.92 ± 0.34 Å, respectively. The final structures were analyzed by Curves 5.3 (19), 3DNA (20), Madbend (21) and MOLMOL (22). The atomic coordinates have been deposited in the Protein Data Bank [PDB ID codes 1ZYF (*hix*-AT), 1ZYG (*hix*-CG) and 1ZYH (*hix*-AG)].

Base pair kinetics

Selective longitudinal relaxation times were measured at increasing concentrations of ammonia ranging from 0 to 0.19 M at 12, 17 and 22°C while maintaining a pH of 8.9–9.0. The water signal was suppressed by the jump-and-return pulse sequence. Interpretation and analysis of the data followed the previously reported method (23).

Fluorescence resonance energy transfer

Half of the single-stranded oligonucleotides were labeled with fluorescein on their 5′ ends through a six-carbon linker (C_6), and their complementary sequences were labeled with 6-carboxytetramethylrhodamine (TAMRA) on their 5′ ends. These and all non-labeled oligonucleotides of the same sequences were purchased from Bioneer Co., Ltd. (Daejeon, Korea). The constructs used for FRET experiments were fluorescein-C_6-5′-TTA TCA AAA ACC ATG GTT TTC AAG AA-3′, TAMRA-5′-TTC TTG AAA ACC ATG GTT TTT GAT AA-3′, fluorescein-C_6-5′-TTA TCA AAA ACC CGG GTT TTC AAG AA-3′, TAMRA-5′-TTC TTG AAA ACC CGG GTT TTT GAT AA-3′, fluorescein-C_6-5′-TTA TCA AAA ACC AGG GTT TTC AAG AA-3′ and TAMRA-5′-TTC TTG AAA ACC CTG GTT TTT GAT AA-3′. Equimolar concentrations of each of the complementary DNA strands in 10 mM Tris–HCl, pH 7.5 (20°C) and 0.1 mM EDTA were incubated at 95°C for 10 min and then slowly cooled to room temperature. Complete annealing was checked by non-denaturing PAGE. All FRET experiments were carried out with 0.5 μM of singly- or doubly-labeled dsDNA. Acquired data were processed as described previously (24).

RESULTS

The mutated Hin binding site, *hix*-AG, is recognized by Hin only if it is supercoiled

EMSAs using Hin and 200 bp linear dsDNA fragments showed that Hin binds to the symmetric *hix* site, which has AT as its central +1/−1 residues (*hix*-AT) (Figure 1A and B). Although the native *hixL* and *hixR* sites have AA sequences at their centers, the symmetric *hix*-AT site has been tested in *in vitro* DNA-binding assays, such as EMSAs and methylation protection assays, and found to bind Hin as well as the wild-type *hix* sites (25). Furthermore, the *hix*-AT sequence exhibits biological activity equivalent to that of the native *hix* site in invertasome formation, and inversion reactions (13).

If the central AT sequence is changed to AG (*hix*-AG), Hin cannot recognize the *hix* site even though the other residues important for sequence-specific contacts between Hin and *hix* are preserved. However, DNA binding by Hin can be recovered by replacing the central AG with CG (*hix*-CG). Consistent with results obtained for linear DNA fragments, our DNase I footprinting experiments using supercoiled plasmid DNA showed that Hin binds to *hix*-AT and *hix*-CG DNAs. However, quite unexpectedly, Hin also bound to supercoiled *hix*-AG with comparable affinity (Figure 1C). A mutated version of the Hin protein (G102A), which does not bind to the *hix* site (26), also did not bind to supercoiled *hix*-AG. This confirms that the protection from DNase I digestion that was observed with wild-type Hin at the *hix*-AG site is not an artifact caused by experimental conditions and/or non-specific binding (data not shown).

hix-AT, *hix*-AG and *hix*-CG have different overall structures

In order to understand the structural basis of the sensitivity of *hix*-AG to supercoiling, we determined and compared the solution structures of three dodecamer DNAs (*hix*-AT, *hix*-AG and *hix*-CG) (Figure 2). The NOE connectivity and chemical shifts of imino protons in the D_2O and H_2O NOESY spectra showed that *hix*-AT, *hix*-AG and *hix*-CG have the expected right-handed helix structures. Also, nearly all of the residues of *hix*-AT and *hix*-CG showed H1′-H2′ scalar couplings larger than 8–9 Hz, indicating that they have C2′-endo sugar puckerings typical of B-form DNA. However, most of the residues in *hix*-AG showed smaller H1′-H2′ scalar

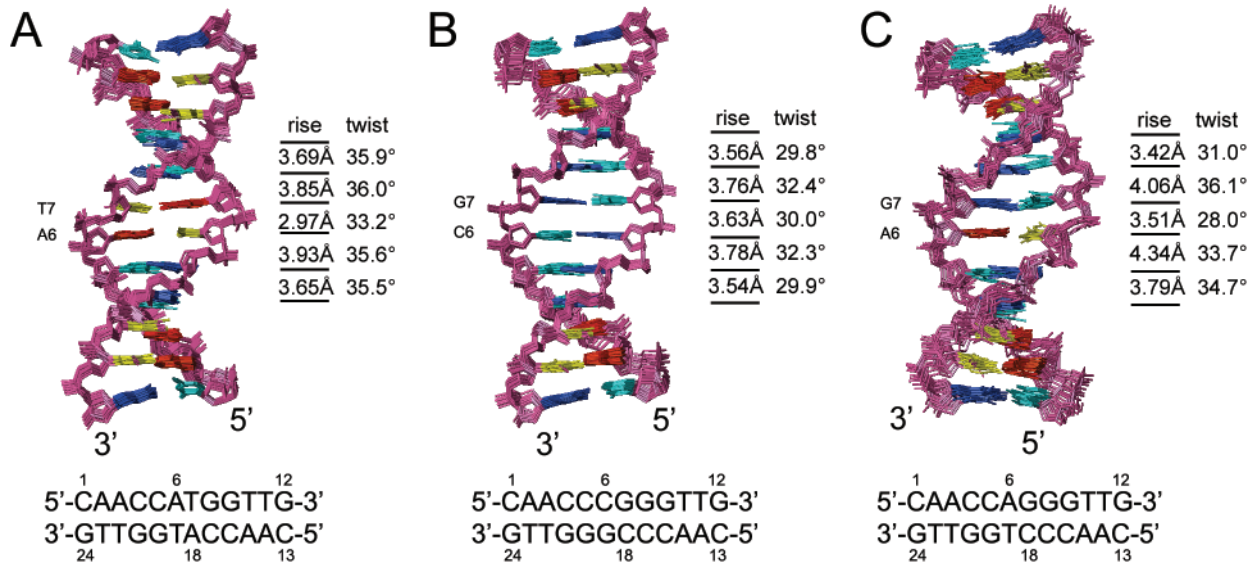

Figure 2. Superimposed overall structures of the *hix* sites. View into the minor groove of (**A**) *hix*-AT (25 structures), (**B**) *hix*-CG (15 structures) and (**C**) *hix*-AG (13 structures). Adenines are colored in red, guanines in blue, cytidines in cyan and thymidines in yellow. Rise and twist are shown for each of the central 5 bp steps.

Table 1. Structure determination statistics

	hix-AT	*hix*-CG	*hix*-AG
Total number of NOE distance restraints	222	205	354
Intra-residue	86	76	159
Sequential residue	94	93	161
Interstrand	42	36	34
Dihedral restraints (β, γ, δ, ε and χ)	116	113	116
Base pair planarity restraints	12	12	12
Total number of restraints	350	330	482
Pairwise r.m.s.d. for all heavy atoms (Å)	0.56 ± 0.29	0.61 ± 0.34	0.92 ± 0.34
r.m.s.d. to the mean structure (Å)	0.65	0.54	0.79
Average NOE violations (Å)	0 (>0.5Å)	0 (>0.5Å)	0 (>0.5Å)
Average dihedral angle violations (degrees)	0 (>5°)	0 (>5°)	0 (>5°)
Mean deviation from covalent geometry			
Bond lengths (Å)	0.007	0.007	0.007
Angles (degrees)	0.9	0.9	1.0
Impropers (degrees)	2	2	2

couplings in a range of 6–8 Hz (data not shown), which suggests that *hix*-AG undergoes a dynamic equilibrium between the C2′- and C3′-endo sugar puckers. Because typical A-form DNA, which has the C3′-endo sugar pucker, shows H1′-H2′ scalar couplings of <2.0 Hz, *hix*-AG appears to spend most of its time in a B-form-like structure rather than an A-form-like structure. A total of 350, 330 and 482 restraints, respectively, for the *hix*-AT, *hix*-CG and *hix*-AG were derived from NMR data and were used for structure calculations to obtain well-converged ensemble structures (Table 1).

The major groove widths of *hix*-AT, *hix*-CG and *hix*-AG were within a ±2 Å boundary of the major groove width of average B-form DNA (27). *hix*-AG showed the largest major groove width (∼14 Å), which is significantly larger than that of *hix*-AT (∼10 Å). The major grooves of *hix*-AT and *hix*-CG had similar depths (∼4 Å), but *hix*-AG had a very shallow (∼1.5 Å) depth in the middle of the sequence. *hix*-AT had a narrow (width, ∼7 Å) and deep (depth, ∼5.3 Å) minor groove, which is similar to that of average B-form DNA, while *hix*-CG had a wide (width, ∼10 Å) and shallow (depth, ∼3.5 Å) minor groove, which is similar to that of average A-form DNA (27). The minor groove of *hix*-AG was of intermediate width and depth, when compared with those of *hix*-AT and *hix*-CG (Figure 2).

hix-AG is partially unwound and stretched

The converged structures of *hix*-AT, *hix*-CG and *hix*-AG showed sequence-dependent structural differences in quantitative helical analyses. Because of the possible inaccuracy of the structure defined for the terminal residues, we assessed only the central 6 bp and their 5 bp steps for each DNA.

The accumulation of rises of central base pair steps from C4–C5 to G8–G9 was 18.1, 18.3 and 19.1 Å for *hix*-AT, *hix*-CG and *hix*-AG, respectively (Figure 2). This increased helical rise could result from a twist. The sum of the twist angles of the base pair steps from C4–C5 to G8–G9 were 163.5° for the *hix*-AG, which is less than that calculated for *hix*-AT by 12.7° (Figure 2). The lack of a twist in *hix*-AG compared with *hix*-AT is consistent with previous analyses of the local helix parameters of high-resolution DNA crystal structures, in which the mean twist angles of AT, CG and AG base pair steps are 33.4 ± 3.5°, 31.1 ± 4.7° and 30.5 ± 4.9°, respectively (28). If we assume the standard A- or B-form DNA structures (27) keep their helical diameter constant upon unwinding, then a decrease in the twist angle of 12.7° could be transformed into an increase of 1.0–1.2 Å in the helical rise. Supporting this assumption, *hix*-AT and *hix*-AG had nearly identical helical diameters, in that the average interstrand P–P distances of base pairs from C4pC5 to G8pG9 were 18.0 ± 0.2 and 18.1 ± 0.2 Å, respectively. Similar mechanism of DNA stretching has been observed in

several DNA complexes, such as those that contain catabolic activator protein (29) or TATA-box binding protein (30). Such DNA-binding proteins can make use of the natural coupling of twist and roll with slide and/or shift to stretch DNA at selected base pair steps.

The accumulated twist angle of *hix*-CG for residues from C4–C5 to G8–G9 was 154.4°, which is even smaller (by 9.1°) than that of *hix*-AG. However, unlike *hix*-AG, *hix*-CG showed no significant increase in the helical rise. It is possible that the increased helical diameter or interstrand P–P distance we observed for *hix*-CG (18.4 ± 0.2 Å) can accommodate the unwinding without further stretching of the DNA.

hix-AG has high potential for deformation

Because partially unwound DNA sites are easily bent (31,32), we sought to determine whether DNA bending differed among *hix*-AG, *hix*-AT and *hix*-CG by assessing their roll, tilt and twist angles (21). Because the distance constraints used in structural calculations cover a relatively short distance range (<6 Å) and thus cannot define a long-range curvature accurately, we included only the central 5 bp steps in our DNA curvature calculations. Both *hix*-AT and *hix*-AG, which exhibited negative global rolls (−8 ± 5° and −10 ± 7°), were bent toward the minor groove by 8 ± 5° and 12 ± 6°, respectively. *hix*-CG, which had a positive roll (8 ± 6°), was bent toward the major groove by 9 ± 5°. Considering that the bending flexibility of generic B-DNA, which was estimated from Monte Carlo simulations using a static bend model, is 5° (33), our results indicate that all three oligonucleotides are only slightly bent and the magnitude of bending of the *hix*-AG is not remarkably different from that of the *hix*-AT or *hix*-CG.

However, statistics of crystal structures of DNA and DNA–protein complexes have demonstrated that AG dinucleotide steps tend to undergo significant translational and tilt changes, while AT and CG dinucleotide steps have essentially no base pair displacement (34). Therefore, we suspected that *hix*-AG might have higher potential of deformation than *hix*-AT or *hix*-CG even though *hix*-AG did not appear to have significant intrinsic curvature. Because the DNA phosphate backbone is negatively charged, electrostatic interactions with monovalent or divalent cations are important in DNA bending, twisting, groove width variation and deformation (35). Furthermore, sequence-directed bending in DNA has been reported as an inducible, not a static, phenomenon (36,37). Thus we investigated the effect of salts on the deformation of 26 bp *hix*-AT and *hix*-AG DNAs, where the change of end-to-end distance was monitored by a change in FRET efficiency (38). Increasing the salt concentration of Na^+, NH_4^+ and Mg^{2+} from 0.0 to 0.5 M augmented the FRET efficiency for all DNAs, *hix*-AT, *hix*-CG and *hix*-AG (Figure 3A–C). Salt-dependent changes in FRET efficiency may result not only from changes in the end-to-end distance, but also from changes in the fluorescence characteristics of the fluorophores; however, the absorbance and fluorescence of rhodamine used here are known to be very stable at least up to 0.5 M NaCl (24). In the case of Mg^{2+}, FRET efficiencies of *hix*-AT, *hix*-CG and *hix*-AG increased so rapidly that no significant differences were observed between them. However, for both Na^+ and NH_4^+, the FRET efficiency of *hix*-AG increased more rapidly than that of the *hix*-AT or *hix*-CG, suggesting that *hix*-AG is more flexible and, therefore, more easily deformed as the salt concentration increases.

Base pair opening of *hix*-AG is very fast

DNA deformation occurs concurrently with base pair opening, and the propensity of base pair opening is also related to the thermodynamics and kinetics of DNA deformation (21,30,39). In order to explore the differential dynamics of the three *hix* sites, we measured the base pair lifetimes of the common G8–C17 base pair using ammonia as a base catalyst (Figure 4A). In a stacked helix, the imino protons are protected from exchange with a base catalyst, but in the presence of higher concentrations of a base catalyst, exchange of imino protons may take place each time a base pair opens. When we consider that the typical base pair lifetimes of A–T and G–C base pairs are 0.5–7 and 4–50 ms, respectively (23), the lifetimes of G8–C20 base pairs measured at 17°C for *hix*-AT (5.0 ms), *hix*-CG (4.4 ms) and *hix*-AG (−2.6 ms) and those values measured at 12°C for *hix*-AT (2.8 ± 3.0 ms), *hix*-CG (12.8 ± 4.6 ms) and *hix*-AG(-7.0 ± 6.4 ms) imply that the central base pairs of *hix*-CG and *hix*-AG are rapidly opened and closed, with *hix*-AG undergoing the fastest local motion. It appears consistent with the previous observation that a

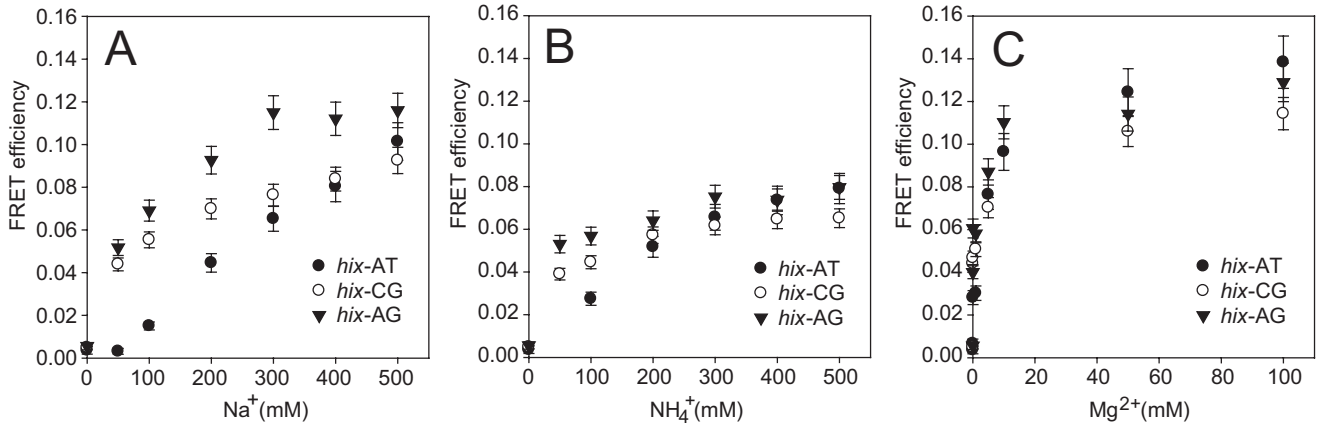

Figure 3. End-to-end distances of *hix*-AT and *hix*-AG. (**A**–**C**) Dependence of FRET efficiency on the concentration of NaCl, NH_4Cl and $MgCl_2$ in the buffer [10 mM Tris–HCl (pH 7.5, 20°C) and 0.1 mM EDTA].

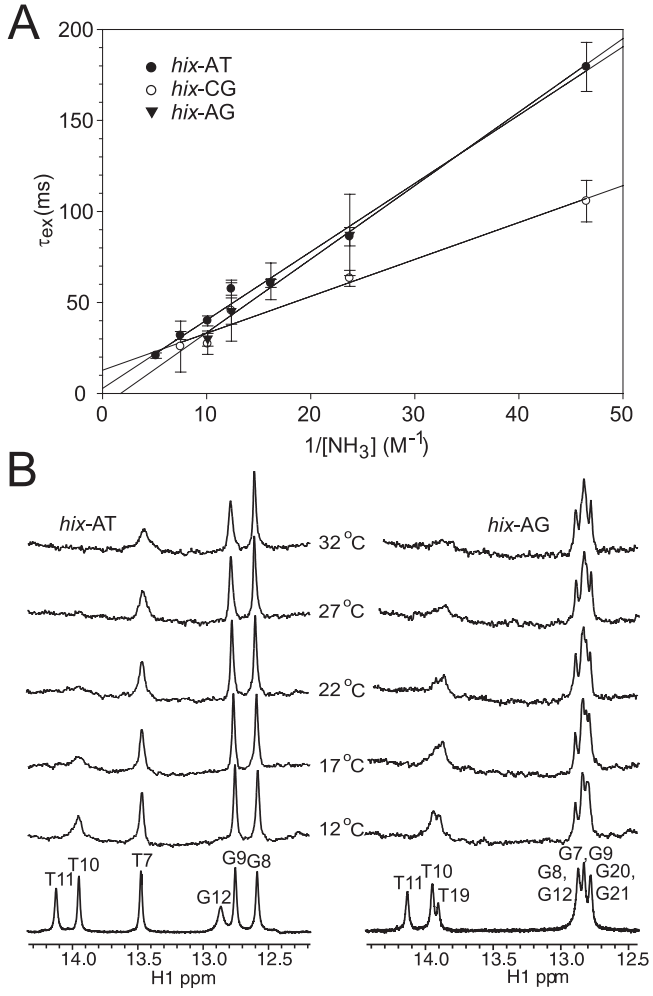

Figure 4. Base pair opening kinetics of *hix*-AT, *hix-CG* and *hix*-AG. (**A**) Exchange time of the G8 imino proton was measured at varying concentrations of base catalyst, ammonia, at pH 8.9, 12°C. Base pair lifetime was calculated by extrapolation to infinite ammonia concentration, [NH_3]. (**B**) Imino spectra of *hix*-AT and *hix*-AG at increasing temperature. For the 17–32°C spectra, the buffer contained 0.136 M NH_3/NH_4^+ (at pH 9.0, [NH_3] = 45 mM) and 100 mM NaCl.

G-C base pair within consecutive G-C base pairs has an unusually short base pair lifetime (40). The opening of the central G8–C17 base pair of *hix*-AG did not seem to follow the simple two-state model (23), and the measured exchange times were not extrapolated to a positive value at an infinite concentration of ammonia. However, we confirmed, by monitoring the central imino proton while increasing the temperature of samples at a given concentration of base catalyst, that *hix*-AG base pair exhibited faster base pair opening kinetics than did the *hix*-AT base pair (Figure 4B).

DISCUSSION

The three mutant *hix* sites (*hix*-AT, *hix*-CG and *hix*-AG) studied here are the same except for one or two base pairs. However, we have shown that their structural and dynamical properties are remarkably different, which may explain the differential binding of Hin to these sites in the presence or absence of supercoiling. Supercoiling confers topological constraints on the local DNA structure. As protein binding induces structural changes in the DNA-binding site, supercoiling should also induce structural changes in the local DNA site where flexibility of the DNA including and surrounding this site would be critical for a response to supercoiling. Supporting this idea, the partially unwound and stretched structure of *hix*-AG shows high potential for deformation and very fast kinetics of base pair opening. Furthermore, in the present study, we have revealed that a single CAG/CTG triplet sequence motif contained in *hix*-AG shows essentially the same characteristics as do multiple CAG/CTG repeats which are associated with several hereditary neuromuscular diseases, including myotonic dystrophy and Huntington's disease; a block of multiple CAG/CTG repeats is present near or within genes associated with such diseases (12). The gel mobility and cyclization kinetics of DNA that contains short tracts of CAG/CTG repeats revealed that the CAG/CTG repeats are intrinsically straight but extremely flexible (41). Also, a stretch of multiple CAG/CTG repeats shows an unusually high affinity for the histone octamer, forming a tight nucleosome (42) in which DNA wraps around a histone core in a left-handed configuration that produces a negative toroidal supercoiling. The free energy of supercoiling for the CAG/CTG repeats calculated by statistical mechanics is only 66% of that of random B-DNA at a length of 10^4 bp (43).

How might the structural and dynamic properties of the CAG/CTG site explain the supercoiling-dependent interaction between Hin and *hix*-AG? There may be a few possible reasons for why *hix*-AG is not bound by Hin when the DNA is relaxed, but is bound by Hin when the DNA is supercoiled. First, the spacing between the half-sites in the *hix* sequence might be critical for DNA inversion, as demonstrated by a mutant *hix* site that contains AAA sequence rather than AA sequence at the center of an otherwise normal *hix* site (13). However, the Hin dimer is flexible enough to bind to both half-sites of *hix* sequences that contain a 2 (wild type), 3 or 5 bp spacer between the half-sites, albeit the following inversion process is aborted (6). The same flexibility has been reported for the γδ resolvase, which shares ~40% amino acid sequence identity with Hin and which binds to three *res* subsites, each with a different spacer length (7, 10 and 16 bp) between two half-sites (44). Therefore, the differential spacing or the helical rise may not be relevant at least with respect to Hin-*hix*-AG binding.

Second, the bending property of *hix*-AG may differ from that of *hix*-AT and *hix*-CG. Several studies on the homologous γδ resolvase (44) and Gin invertase (45) and preliminary results of circular permutation assays on the Hin recombinase suggest that the *hix* site should be bent toward the major groove upon Hin binding (6). We showed that all three *hix* sites are similarly bent with a magnitude ranging from 8 to 12°. However, *hix*-AT and *hix*-AG are bent toward the minor groove, which is opposite to the expected orientation of the bending in the Hin-bound *hix* site. Also, kinetics of base pair opening and fluctuations of roll and tilt indicated that *hix*-AG is significantly more disordered than *hix*-AT. Therefore, a great entropy loss due to the constraints imposed by complex formation as well as additional energy required for inverting the orientation of bending may explain the unfavorable

binding between Hin and relaxed *hix*-AG site. Effect of supercoiling on a local DNA structure has been shown to be mimicked by a nick which is known to hardly alter the bending flexibility but to substantially increase twist flexibility (46,47). Our FRET data and the preferred occurrence of CAG/CTG triplet at the dyad of nucleosome suggest that CAG/CTG triplet has high twist and bending flexibility (48). Combined together with this intrinsic flexibility of CAG/CTG site, extrinsic twist flexibility provided by supercoiling would facilitate further unwinding of *hix*-AG, which shall increase roll and thus change the orientation of bending through strong negative correlation between twist and roll (28,34). This structural change will reduce the energetic cost of Hin binding. CAG/CTG site may gain flexibility by supercoiling because of its high susceptibility to deformation, on the other hand, surrounding DNA sites involved in the sequence-specific contacts between Hin and *hix* might become less flexible due to the structural constraints imposed by supercoiling, which reduces the overall entropy loss of binding between Hin and supercoiled *hix*-AG.

The strategy underlying the above explanations could be generalized as follows: supercoiling affects predominantly the DNA site having high intrinsic flexibility, and it switches the local DNA structure from an inefficient conformation for protein interaction to an efficient one, or vice versa. An example of this notion is the *mdm2* promoter, which is responsive to changes in superhelicity (4). Unlike other binding sites for the tumor suppressor protein p53, the *mdm2* promoter has two consensus p53 binding sites separated by a 17 bp spacer that contains a CAG/CTG in the middle of the sequence. Because a p53 tetramer binds to either a single consensus sequence or tandem sequences and stacks one on top of the other (49), the inhibitory effect of supercoiling on sequence-specific binding by p53 could be rationalized by flexibility of CAG/CTG site of the spacer that could determine the distance and relative orientation between the two consensus p53 binding sites.

Similar strategies can be found in supercoiling-sensitive *E.coli* promoters too, but they appear to adopt different sequence motifs for responding to changes of superhelicity (Supplementary Data). For eukaryotic promoters, analysis of a large set of human RNA polymerase II promoters has revealed a periodic occurrence of the CAG/CTG steps in the region of promoters downstream from the transcription start site (50). Because, in the polymerase–promoter complex, the polymerase topologically constrains 1–2 left-handed supercoiling (2), this suggests that the structural changes triggered at the periodic CAG/CTG steps by local supercoiling induce the initial open complex formation in a manner reminiscent of the DNA when it is packaged in a nucleosome.

SUPPLEMENTARY DATA

Supplementary Data are available at NAR Online.

ACKNOWLEDGEMENTS

This work was supported by the National Creative Research Initiative from the Ministry of Science and Technology of the Republic of Korea. Funding to pay the Open Access publication charges for this article was provided by the National Creative Research Initiative from the Ministry of Science and Technology, Korea.

Conflict of interest statement. None declared.

REFERENCES

1. Dorman,C.J. (1996) Flexible response: DNA supercoiling, transcription and bacterial adaptation to environmental stress. *Trends Microbiol.*, **4**, 214–216.
2. Travers,A. and Muskhelishvili,G. (2005) DNA supercoiling—a global transcriptional regulator for enterobacterial growth? *Nature Rev. Microbiol.*, **3**, 157–169.
3. Peter,B.J., Arsuaga,J., Breier,A.M., Khodursky,A.B., Brown,P.O. and Cozzarelli,N.R. (2004) Genomic transcriptional response to loss of chromosomal supercoiling in *Escherichia coli*. *Genome Biol.*, **5**, R87.
4. Kim,E., Rohaly,G., Heinrichs,S., Gimnopoulos,D., Meissner,H. and Deppert,W. (1999) Influence of promoter DNA topology on sequence-specific DNA binding and transactivation by tumor suppressor p53. *Oncogene*, **18**, 7310–7318.
5. Silverman,M. and Simon,M. (1980) Phase variation: genetic analysis of switching mutants. *Cell*, **19**, 845–854.
6. Glasgow,A.C., Bruist,M.F. and Simon,M.I. (1989) DNA-binding properties of the Hin recombinase. *J. Biol. Chem.*, **264**, 10072–10082.
7. Feng,J.A., Johnson,R.C. and Dickerson,R.E. (1994) Hin recombinase bound to DNA: the origin of specificity in major and minor groove interactions. *Science*, **263**, 348–355.
8. Chiu,T.K., Sohn,C., Dickerson,R.E. and Johnson,R.C. (2002) Testing water-mediated DNA recognition by the Hin recombinase. *EMBO J.*, **21**, 801–814.
9. Lim,H.M., Hughes,K.T. and Simon,M.I. (1992) The effects of symmetrical recombination site hixC on Hin recombinase function. *J. Biol. Chem.*, **267**, 11183–11190.
10. Johnson,R.C. and Bruist,M.F. (1989) Intermediates in Hin-mediated DNA inversion: a role for Fis and the recombinational enhancer in the strand exchange reaction. *EMBO J.*, **8**, 1581–1590.
11. Lim,H.M., Lee,H.J., Jaxel,C. and Nadal,M. (1997) Hin-mediated inversion on positively supercoiled DNA. *J. Biol. Chem.*, **272**, 18434–18439.
12. Paulson,H.L. and Fischbeck,K.H. (1996) Trinucleotide repeats in neurogenetic disorders. *Annu. Rev. Neurosci.*, **19**, 79–107.
13. Johnson,R.C. and Simon,M.I. (1985) Hin-mediated site-specific recombination requires two 26 bp recombination sites and a 60 bp recombinational enhancer. *Cell*, **41**, 781–791.
14. Delaglio,F., Grzesiek,S., Vuister,G.W., Zhu,G., Pfeifer,J. and Bax,A. (1995) NMRPipe: a multidimensional spectral processing system based on UNIX pipes. *J. Biomol. NMR*, **6**, 277–293.
15. Borgias,B.A. and James,T.L. (1989) Two-dimensional nuclear Overhauser effect: complete relaxation matrix analysis. *Methods Enzymol.*, **176**, 169–183.
16. Delaglio,F., Wu,Z. and Bax,A. (2001) Measurement of homonuclear proton couplings from regular 2D COSY spectra. *J. Magn. Reson.*, **149**, 276–281.
17. Schwieters,C.D., Kuszewski,J.J., Tjandra,N. and Clore,G.M. (2003) The Xplor-NIH NMR molecular structure determination package. *J. Magn. Reson.*, **160**, 65–73.
18. Kuszewski,J., Schwieters,C. and Clore,G.M. (2001) Improving the accuracy of NMR structures of DNA by means of a database potential of mean force describing base–base positional interactions. *J. Am. Chem. Soc.*, **123**, 3903–3918.
19. Lavery,R. and Sklenar,H. (1988) The definition of generalized helicoidal parameters and of axis curvature for irregular nucleic acids. *J. Biomol. Struct. Dyn.*, **6**, 63–91.
20. Lu,X.J. and Olson,W.K. (2003) 3DNA: a software package for the analysis, rebuilding and visualization of three-dimensional nucleic acid structures. *Nucleic Acids Res.*, **31**, 5108–5121.
21. Strahs,D. and Schlick,T. (2000) A-Tract bending: insights into experimental structures by computational models. *J. Mol. Biol.*, **301**, 643–663.
22. Koradi,R., Billeter,M. and Wuthrich,K. (1996) MOLMOL: a program for display and analysis of macromolecular structures. *J. Mol. Graph.*, **14**, 51–55, 29–32.

23. Gueron,M. and Leroy,J.L. (1995) Studies of base pair kinetics by NMR measurement of proton exchange. *Methods Enzymol*., **261**, 383–413.
24. Toth,K., Sauermann,V. and Langowski,J. (1998) DNA curvature in solution measured by fluorescence resonance energy transfer. *Biochemistry*, **37**, 8173–8179.
25. Hughes,K.T., Youderian,P. and Simon,M.I. (1988) Phase variation in *Salmonella*: analysis of Hin recombinase and hix recombination site interaction *in vivo*. *Genes Dev*., **2**, 937–948.
26. Lee,H.J., Lee,S.Y., Lee,H. and Lim,H.M. (2001) Effects of dimer interface mutations in Hin recombinase on DNA binding and recombination. *Mol. Genet. Genomics*, **266**, 598–607.
27. Saenger,W. (1984) *Principles of Nucleic Acid Structure*. Springer-Verlag, NY .
28. Gorin,A.A., Zhurkin,V.B. and Olson,W.K. (1995) B-DNA twisting correlates with base-pair morphology. *J. Mol. Biol*., **247**, 34–48.
29. Schultz,S.C., Shields,G.C. and Steitz,T.A. (1991) Crystal structure of a CAP–DNA complex: the DNA is bent by 90 degrees. *Science*, **253**, 1001–1007.
30. Kim,Y., Geiger,J.H., Hahn,S. and Sigler,P.B. (1993) Crystal structure of a yeast TBP/TATA-box complex. *Nature*, **365**, 512–520.
31. Kahn,J.D., Yun,E. and Crothers,D.M. (1994) Detection of localized DNA flexibility. *Nature*, **368**, 163–166.
32. Ramstein,J. and Lavery,R. (1988) Energetic coupling between DNA bending and base pair opening. *Proc. Natl Acad. Sci. USA*, **85**, 7231–7235.
33. Nathan,D. and Crothers,D.M. (2002) Bending and flexibility of methylated and unmethylated EcoRI DNA. *J. Mol. Biol*., **316**, 7–17.
34. Olson,W.K., Gorin,A.A., Lu,X.J., Hock,L.M. and Zhurkin,V.B. (1998) DNA sequence-dependent deformability deduced from protein–DNA crystal complexes. *Proc. Natl Acad. Sci. USA*, **95**, 11163–11168.
35. McFail-Isom,L., Sines,C.C. and Williams,L.D. (1999) DNA structure: cations in charge? *Curr. Opin. Struct. Biol*., **9**, 298–304.
36. Laundon,C.H. and Griffith,J.D. (1987) Cationic metals promote sequence-directed DNA bending. *Biochemistry*, **26**, 3759–3762.
37. Stefl,R., Wu,H., Ravindranathan,S., Sklenar,V. and Feigon,J. (2004) DNA A-tract bending in three dimensions: solving the dA4T4 vs. dT4A4 conundrum. *Proc. Natl Acad. Sci. USA*, **101**, 1177–1182.
38. Lakowicz,J.R. (1983) *Principles of Fluorescence Spectroscopy*. Plenum Press, NY.
39. Kim,J.L., Nikolov,D.B. and Burley,S.K. (1993) Co-crystal structure of TBP recognizing the minor groove of a TATA element. *Nature*, **365**, 520–527.
40. Dornberger,U., Leijon,M. and Fritzsche,H. (1999) High base pair opening rates in tracts of GC base pairs. *J. Biol. Chem*., **274**, 6957–6962.
41. Chastain,P.D. and Sinden,R.R. (1998) CTG repeats associated with human genetic disease are inherently flexible. *J. Mol. Biol*., **275**, 405–411.
42. Wang,Y.H. and Griffith,J. (1995) Expanded CTG triplet blocks from the myotonic dystrophy gene create the strongest known natural nucleosome positioning elements. *Genomics*, **25**, 570–573.
43. Gellibolian,R., Bacolla,A. and Wells,R.D. (1997) Triplet repeat instability and DNA topology: an expansion model based on statistical mechanics. *J. Biol. Chem*., **272**, 16793–16797.
44. Hatfull,G.F., Noble,S.M. and Grindley,N.D. (1987) The gamma delta resolvase induces an unusual DNA structure at the recombinational crossover point. *Cell*, **49**, 103–110.
45. Mertens,G., Klippel,A., Fuss,H., Blocker,H., Frank,R. and Kahmann,R. (1988) Site-specific recombination in bacteriophage Mu: characterization of binding sites for the DNA invertase Gin. *EMBO J*., **7**, 1219–1227.
46. Jordi,B.J., Owen-Hughes,T.A., Hulton,C.S. and Higgins,C.F. (1995) DNA twist, flexibility and transcription of the osmoregulated proU promoter of *Salmonella typhimurium*. *EMBO J*., **14**, 5690–5700.
47. Zhang,Y. and Crothers,D.M. (2003) High-throughput approach for detection of DNA bending and flexibility based on cyclization. *Proc. Natl Acad. Sci. USA*, **100**, 3161–3166.
48. Godde,J.S. and Wolffe,A.P. (1996) Nucleosome assembly on CTG triplet repeats. *J. Biol. Chem*., **271**, 15222–15229.
49. Stenger,J.E., Tegtmeyer,P., Mayr,G.A., Reed,M., Wang,Y., Wang,P., Hough,P.V. and Mastrangelo,I.A. (1994) p53 oligomerization and DNA looping are linked with transcriptional activation. *EMBO J*., **13**, 6011–6020.
50. Pedersen,A.G., Baldi,P., Chauvin,Y. and Brunak,S. (1998) DNA structure in human RNA polymerase II promoters. *J. Mol. Biol*., **281**, 663–673.